Bulletin of the Geological Society of Finland, Vol. 95, 2023, pp 35–46 https://doi.org/10.17741/bgsf/95.1.003

Clay mineral and Nd, Pb, and Sr isotope provenance of a MIS 4-3 sediment record from the Lomonosov Ridge, central Arctic Ocean

Raisa Alatarvas*, Ninna Immonen and Kari Strand

Oulu Mining School, University of Oulu, 90014 Oulun yliopisto, Finland

VERTAISARVIOITU
KOLLEGIALT GRANSKAD
PEER-REVIEWED
www.tsv.fi/tunnus

Abstract

Modern techniques for detrital mineral provenance were applied to sediment core 96/12-1pc from the Lomonosov Ridge in the central Arctic Ocean. The techniques include quantitative clay mineralogy analysis combined with determination of Nd, Pb, and Sr isotopes from clay fraction. The clay mineral assemblage and the isotope signatures depict distinct changes during the Marine Isotope Stage (MIS) 4-3 transition corresponding to the Middle Weichselian deglaciation. This transition is characterised by a homogenous, 48 cm thick, dark grey, silty clay layer with a distinctive IRD concentration, forming a prominent marker bed for the central Arctic Ocean sediments. The elevated smectite and kaolinite contents in the transitional interval are possible weathering products of the Siberian basaltic rocks, such as the Putorana Plateau, feeding the shelves of the Kara Sea and the western Laptev Sea. The Nd and Sr isotope values are compatible with input from the basaltic rocks and fall within the isotopic range of sediments from these shelves. The abrupt changes in the Nd, Pb and Sr isotopic data from the distinct grey layer attributed to the MIS 4-3 transition likely mark a pronounced deglaciation event. An increase in coarse debris in the grey layer indicates a change in the sedimentation regime with a strong iceberg rafting component. This change may also be related to a sudden release of meltwater from a large ice-dammed lake in the northern Siberia.

Keywords: Lomonosov Ridge, Arctic Ocean, marine sediments, Middle Weichselian glaciation, clay mineralogy, Nd-Sr-Pb isotopes

*Corresponding author (email: raisa.alatarvas@oulu.fi)

Editorial handling: Pertti Sarala (pertti.sarala@oulu.fi)

1. Introduction

The disintegration of the Middle Weichselian Eurasian ice sheet and the discharge of a large proglacial lake during deglaciation event in the Marine Isotope Stage (MIS) 4-3 transition have been studied during the past decades (Mangerud et al. 2001, 2004; Krinner et al. 2004; Spielhagen et al. 2004; Svendsen et al. 2004). A distinct grey sediment layer with abundant ice-rafted debris (IRD) has been found in multiple cores from the eastern and central Arctic Ocean (Jakobsson et al. 2000, 2001; Vogt et al. 2001; Spielhagen et al. 2004; Dong et al. 2022). According to the existing stratigraphy, this layer was deposited during the transition from glacial (MIS 4) to interglacial (MIS 3) conditions and forming a prominent Middle Weichselian marker bed for the Arctic Ocean sediments (Jakobsson et al. 2000, 2001; Vogt et al. 2001; Spielhagen et al. 2004; Löwemark et al. 2008). Variations in deep-sea sediments can show changes in the transport pathways related to the history of circulation, sea ice, and icebergs (cf. Wahsner et al. 1999). The current understanding is that under interglacial conditions, such as the present-day, sediments are delivered to the central Arctic Ocean primarily by sea-ice drift from the Eurasian and the American Arctic margins, while during glacial/deglacial intervals, material was largely provided by icebergs and meltwater (e.g., Darby 2003, 2014; Polyak et al. 2010; Darby et al. 2011). According to Clark & Hanson (1983), glacial ice is primarily responsible for the transportation of coarser sediment, and sea ice may be the major source of finer sediment in the central Arctic Ocean.

The clay mineralogy of the central Arctic Ocean sediments has been widely used to identify sediment source areas (Stein et al. 1994; Wahsner et al. 1999; Kalinenko 2001; Viscosi-Shirley et al. 2003; Vogt & Knies 2008; Strand et al. 2008; Krylov et al. 2008, 2014). The radiogenic neodymium (Nd), lead (Pb), and strontium (Sr) isotopes have been applied in sediment provenance tracing and transport mechanism reconstructions in the Arctic region (Tütken et al. 2002; Fagel et al. 2014; Li et al. 2023). This present research offers information on how the clay mineral content and the isotope signatures of the central Arctic Ocean sediments correspond to the deglaciation event during the MIS 4-3 transition. In this study, we investigated the clay mineralogy and the Nd, Pb, and Sr isotopes from the Late Pleistocene sediment record of core 96/12-1pc from the Lomonosov Ridge. The core consists of alternating clay to silty clay sediments with prominent intervals of silt to fine sand size material. The clay fraction is characteristic for meltwater pulses related to deglaciation events and can be transported in varying degree by ocean currents over long distances into the deep ocean basins (cf. Wahsner et al. 1999). Clay-size fraction was selected for the present study due to its high availability in the study material and suitability to both clay mineral and isotope analyses with minimal grain size effects on the isotope systematics (e.g., Tütken et al. 2002; Fagel et al. 2014). Combining our results with published data, we evaluated the provenances and transportation of these detrital sediments in the central Arctic Ocean. The results from this study can be applied in further evaluation of the Arctic ice sheet and circulation history.

2. Geological background

The Lomonosov Ridge is interpreted as a continental fragment/crust that extends 1700 km from the north of Greenland, across the North Pole, to the central Siberian continental shelf, separating the Arctic Ocean into the Eurasian Basin and the Amerasian Basin (Jokat & Ickrath 2015) (Fig. 1). The Arctic Ocean is a relatively enclosed ocean as it has limited connections to the Atlantic and Pacific Oceans via the Fram Strait and Bering Strait, respectively. There are two major wind-driven surface-water circulation systems in the Arctic Ocean: the Beaufort Gyre flowing clockwise in the Amerasian Basin, and the Transpolar Drift in the Eurasian Basin flowing towards the Fram Strait (Schoster et al. 2000; Adler et al. 2009) (Fig. 1). These currents transport surface water masses with

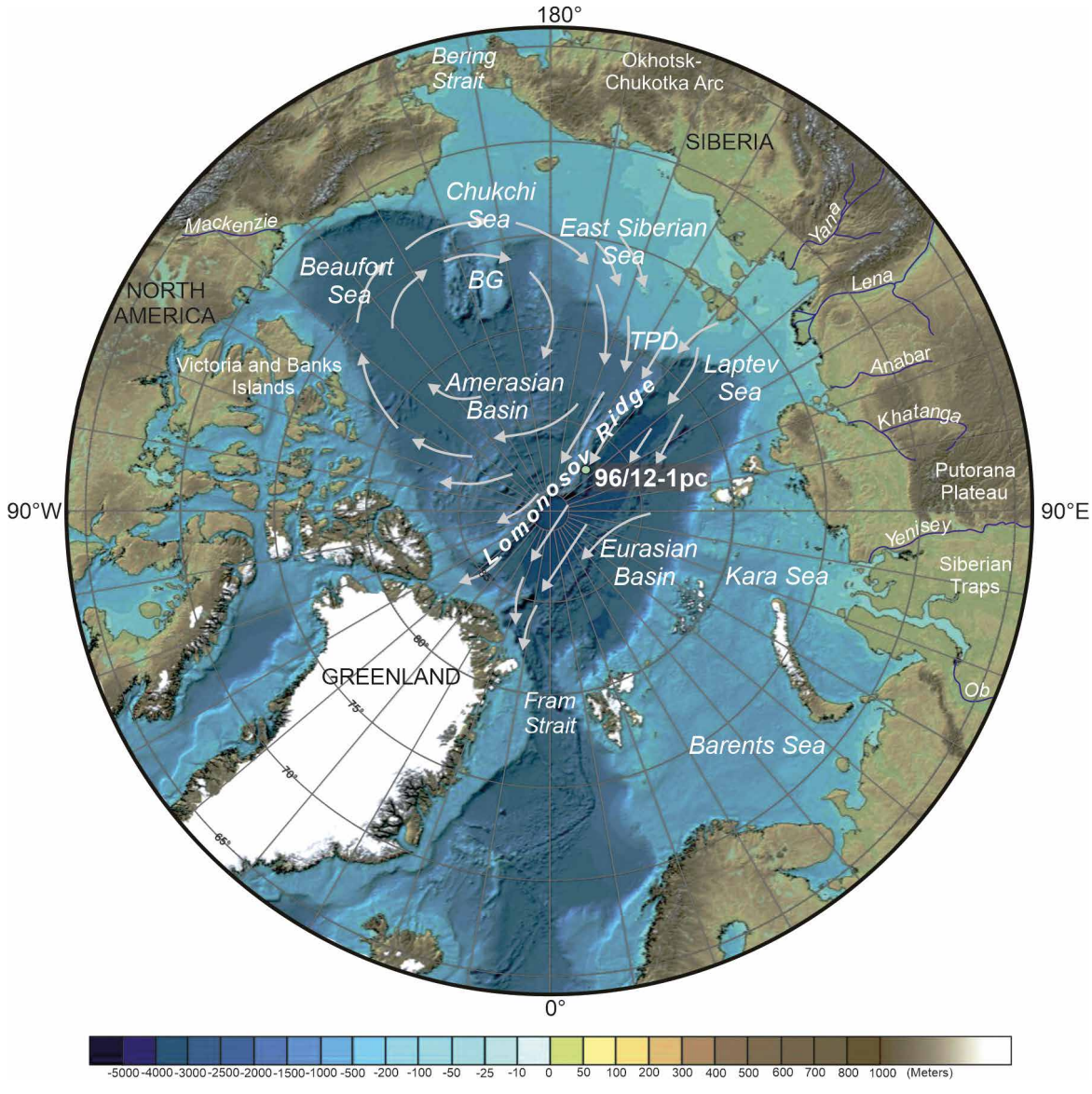

Figure 1. Map of the Arctic Ocean with the location of core 96/12-1pc on the Lomonosov Ridge (modified from Jakobsson et al. 2008). Two major surface-water circulations, the Beaufort Gyre (BG) and the Transpolar Drift (TPD) are indicated by grey arrows (adapted from AMAP 1998).

sea-ice and/or icebergs along with the entrained terrigenous sediments. The Eurasian side provides minerals, including e.g., amphibole, pyroxene and illite, while the Amerasian side mainly provides dolomite and kaolinite (Krylov et al. 2008; Kaparulina et al. 2016). Lower Nd and Pb ratios derive from the North American margin, and higher Nd and Pb ratios from the Eurasian margin (Fagel et al. 2014; Li et al. 2023). The Sr ratios vary within the Eurasian margin sources (Li et al. 2023).

3. Materials and methods

3.1. Sediment core

A 722 cm long piston core 96/12-1pc was recovered from the water depth of 1003 m during the Arctic Ocean-96 expedition (AO96) from the crest of the Lomonosov Ridge (144°46'22"E, 87°05'51"N; Fig. 1) (Jakobsson et al. 2000, 2001). No obvious indications of erosion of the sea-bottom were observed at the core site. The core location in the interaction area of sea-ice transported by the Transpolar Drift and the Beaufort Gyre (Fig. 1) is suitable for recording changes in sedimentary inputs from both the Eurasian and North American margin. The lithostratigraphic description of the core is based on Jakobsson et al. (2000, 2001). From 722 to 193 cm below sea floor (bsf), the core consists of medium to dark brown clays characterised by overall high content of manganese, common bioturbation, and fine particle size. A coarser-grained, light grey-brown, sandy clay between 193 and 186 cmbsf grades to an olive to light brown clay at 186 to 163 cmbsf (Fig. 2). The latter unit is overlain with a sharp contact by a homogenous, dark grey, 48 cm thick, silty clay layer between 163 and 115 cmbsf. The uppermost 115 cmbsf of the core consist of light brown to light yellowish-brown, mottled clayey silt with faint horizontal banding.

An age model based on nannofossil biostratigraphy and Mn cyclicity has been established by Jakobsson et al. (2000) for the upper 220 cmbsf of the core (Fig. 2). According to this approximative age model, the core extends back to ca. 860 ka.

3.2. Clay fraction analyses

3.2.1. Sample preparation

Oriented clay slides were prepared from 3 g of sediment from 47 samples collected at 2–3 cm intervals between 93 and 206 cmbsf (Fig. 2). Distilled water was added to the samples and stirred with a glass rod until they went into suspension. This mixture was centrifuged for 1 minute (1000 rpm) to separate the clay in suspension from the coarser-grained sediment (> 2 μm). The suspension was then transferred to a clean centrifuge tube and centrifuged for 15 minutes (1000 rpm) to settle the clay fraction to the bottom of the tube. The liquid was carefully decanted away, and the clay samples were smeared onto glass slides for the XRD analyses, while the remaining clay material was retained for further analyses. Three different slides were made from each sample; air dried (normal), heated, and ethylene glycol treated. The samples were placed in a drying oven at 60 °C for 2 hours, and the heated samples were then placed in the oven at 550 °C for additional 2 hours, which caused the kaolinite structure to collapse (Hardy & Tucker 1998). Ethylene glycol treated samples were put in a desiccator that was placed in the oven overnight at 60 °C. The ethylene glycol causes smectite to expand its basal spacing from 10 Å to about 17 Å, which makes it recognisable in a diffractogram (Velde 1992).

3.2.2. XRD analysis

X-ray diffraction (XRD) was carried out at the Centre for Material Analysis (CMA), University of Oulu, Finland. The diffractograms were recorded by a Siemens D 5000 diffractometer with a fixed divergence slit (FDS), and copper radiation (40 kV, 40 mA) at angles ranging from 2° to 32° 2θ (0.02° 2θ per second). XRD was performed on oriented clay samples according to Hardy & Tucker (1988) and Moore & Reynolds (1997). MacDiff freeware version 4.2.5 was used to quantify the clay minerals, which were subsequently used to calculate percentages using weighting factors (Biscaye 1965). Peak correction with quartz, smoothing of counts and subtraction of the baseline were done before the analysis. Since no internal standards were available, the precise accuracy of this procedure is not known, but the quantitative analyses justify interpretations of fluctuations around ± 2 %.

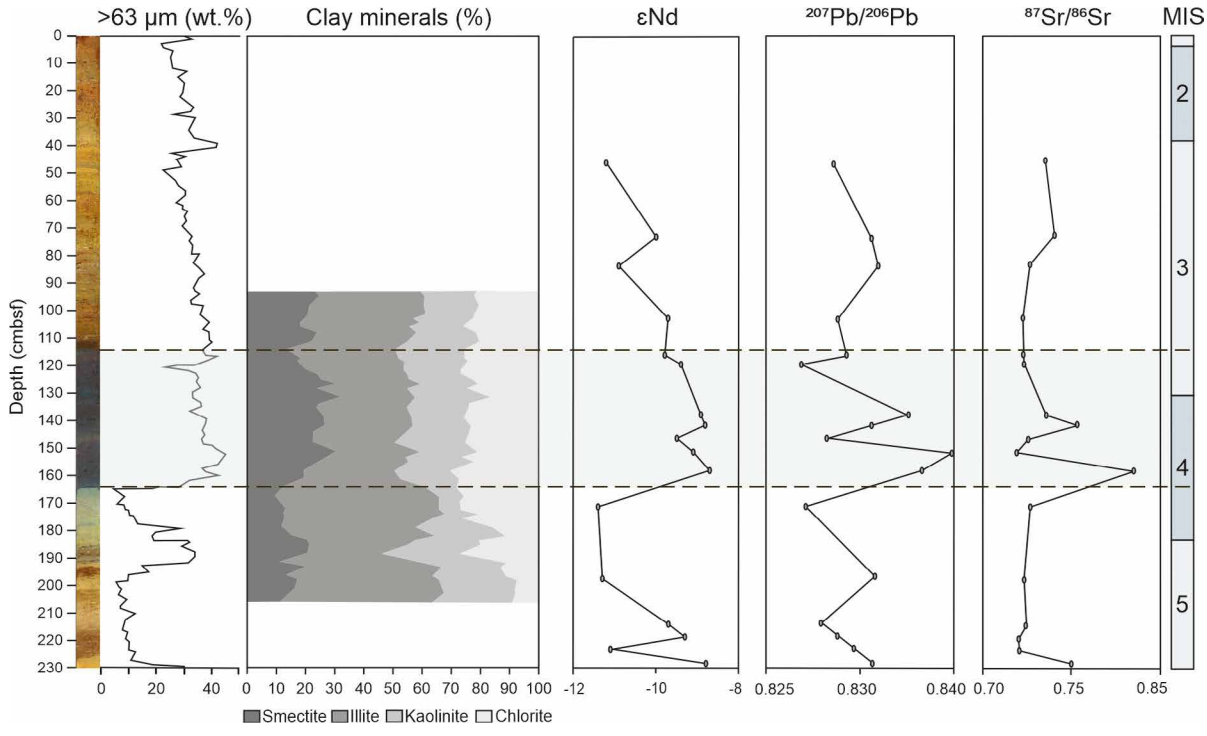

Figure 2. Results of the analyses performed on the clay fraction from core 96/12-1pc: relative content of clay minerals (smectite, illite, kaolinite, and chlorite); εNd, $^{207}Pb/^{206}Pb$, and $^{87}Sr/^{86}Sr$. Distribution of the > 63 µm fraction content adapted from Jakobsson et al. (2001) is plotted next to the digital core image adapted from Jakobsson et al. (2000). The grey layer (115-163 cmbsf) is shown with dashed lines. Position of Marine Isotope Stages (MIS) is adapted from Jakobsson et al. (2001).

3.2.3. Nd, Pb, and Sr isotopic analysis

A total of 17 clay fraction samples were used for the measurements of Nd, Pb, and Sr isotope compositions (Fig. 2). Sample preparation and analyses were carried out at the Geological Survey of Finland, Espoo. Approximately 200 mg of a clay sample was leached with 0.1N HCl in an ultrasonic bath to remove any authigenic material, such as biogenic carbonates and hydrated iron oxides. The samples were then carefully washed several times with distilled water. During the leaching process, the samples lost up to 70 % of their weight. Therefore, more sample material was used for leaching to get ~100 mg sample for digestion. The residues of the leached samples were digested with concentrated $HF+HNO_3+HClO_4$ (3:1:1) in Parr bombs for seven days at 200 °C. The fluorides were evaporated twice with a small amount of concentrated HNO_3. To get a clear solution, the samples in Parr bombs were further digested in an oven for 96 hours/200°C in 2.5 ml of 6.2 N HCl. For the Pb, Sr and Nd concentration analyses, ~1/10 weighed splits were separated and evaporated.

For isotope ratio measurements, Pb was isolated using an AG1-X8 anion exchange resin in HBr environment, and all the washing acids were collected for Sr and Nd purification purposes. Then, Sr and REEs were eluted by using an AG50-X8 cation exchange resin in a HCl environment. From the REE fraction, Nd was eluted using HDEHP-coated (hexyl di-ethyl hydrogen phosphate) Teflon powder as the ion exchange medium in a dilute HCl environment (Richard et al. 1976). For isotope ratio measurements, the sample amounts needed were determined from the measured concentrations and the sediment amount that finally went through the elemental elution processes. Deionised water

with a resistivity of ≥18.2 MΩ·cm was used in the digestion and elemental separation processes, and all the used acids were either single or double-distilled (sub-boiling), depending on the initial acid purity class. Only Teflon vials were used during the digestion and column separation.

The Nd isotope analysis was performed using VG Sector 54 thermal ionisation mass spectrometer (TIMS). Nd isotope ratios were measured using Ta-Re triple filaments in a dynamic mode and $^{143}Nd/^{144}Nd$ ratios were normalised to $^{146}Nd/^{144}Nd$=0.7219. Repeated analyses of the La Jolla Nd standard during the measurements gave $^{143}Nd/^{144}Nd$ of 0.511858 ± 0.000015 (mean and external 2σ error of 12 measurements). The reported external error in the $^{143}Nd/^{144}Nd$ is 0.005 %. The εNd (T= 0 Ma) was calculated using the current chondritic (CHUR) value of $^{143}Nd/^{144}Nd$ = 0.51264 (DePaolo & Wasserburg 1976). The maximum error in the εNd values is ± 0.5 ε-units. The total procedural blank for Nd has usually been < 0.3 ng.

Sr and Pb isotope analyses were carried out using a standard liquid sample introduction system involving a 50µl meinhart nebuliser, a DSN, and a Multi-Collector Inductively Coupled Plasma Mass Spectrometer (Nu InstrumentsTM) at low mass resolution (Δm/m = 400). The isotopic measurements were performed in a static mode using five faraday detectors and 10 blocks of 12 integrations of approximately 5 s. The Sr samples were diluted down to 80 ppb Sr. The standard reference material NBS987, diluted down to 50 ppb Sr, was also used to monitor the precision and accuracy of the measurements at the beginning and the end of every session. The obtained average of 0.71027 ± 0.00002 (n=6, 1sd) for the $^{87}Sr/^{86}Sr$ ratio was close to the NBS987 standard $^{87}Sr/^{86}Sr$ = 0.71034 ± 0.00026. The Pb samples were diluted to 40 ppb Pb. To correct for the mass discrimination effect produced during the analysis, the data were bracketed with the NBS981 standards giving average values of $^{206}Pb/^{204}Pb$ (16.93258 ± 0.00276), $^{207}Pb/^{204}Pb$ (15.48618 ± 0.00257), and $^{208}Pb/^{204}Pb$ (36.68144 ± 0.00852) (n=4, 1sd), which are close to the recommended values (Yuan et al. 2016). The obtained averages of 0.91458 ± 0.00001 (n=4, 2sd) for the $^{207}Pb/^{206}Pb$ and 2.16631 ± 0.00015 (n=4, 2sd) for the $^{208}Pb/^{206}Pb$ ratios were close to the NBS981 standards 0.91464 ± 0.00033 and 2.1681 ± 0.0008, respectively.

4. Results

4.1. Clay minerals

The clay minerals of the studied samples are presented by the relative content of smectite, illite, kaolinite, and chlorite (Fig. 2). The detailed results are presented in the Supplementary Table 1 (Electronic Appendix A). From ~206 cmbsf to the lowermost part of the grey layer (163 cmbsf) the smectite content is < 20 %. There is a notable increasing trend in smectite content upward the grey layer with values up to 32 %. In the upper part of the grey layer, from ~126 to 115 cmbsf, the smectite values show a decreasing trend with the lowest number being 13 %. Above the grey layer (upward from 115 cmbsf), the smectite values increase up to 25 %. Illite content is relatively high (up to 56 %) below the grey layer and upward from 163 cmbsf the values decrease within the layer, with the lowest value being 25 %. Above the grey layer the illite values show an increasing trend with values up to 41 %. Kaolinite content fluctuates between 206 and 163 cmbsf, having the lowest values (7–12 %) just below the grey layer. The increased kaolinite content (up to 24 %) upward from 163 cmbsf corresponds to the lithological change into the grey layer interval. There is a slight decrease in kaolinite content above the grey layer (upward from 115 cmbsf). Chlorite content show notable variations (7–27 %) below the grey layer and within the layer (163–115 cmbsf) the values vary between 20 and 30 %. Above the grey layer the chlorite values have an average of 22 %.

Table 1. The average isotopic values of the studied sediment intervals.

Depth (cmbsf)	εNd ($\bar{x}$)	$^{207}Pb/^{206}Pb$ ($\bar{x}$)	$^{87}Sr/^{86}Sr$ ($\bar{x}$)
43-115	-10.5	0.8322	0.7313
115-163	-9.2	0.8342	0.7376
163-229	-10.3	0.8316	0.7276

4.2. Isotopic composition

The detailed results from the Nd, Pb and Sr isotope analyses are presented in the Supplementary Table 2 (Electronic Appendix B). All the measured isotopic values show distinct excursions from their general trends between 163 and 115 cmbsf, corresponding to the grey sediment layer (Fig. 2). The samples below the grey sediment layer (from 229 to 163 cmbsf), show decreasing trends in the examined isotopic values (Fig. 2). The εNd values vary between -8.8 and -11.4, $^{207}Pb/^{206}Pb$ values between 0.8281 and 0.8338, and $^{87}Sr/^{86}Sr$ values between 0.7201 and 0.7498. In the grey layer sediments (163–115 cmbsf), the examined isotopic values vary highly after an abrupt increase to their maximum values. The εNd values range from -9.8 to -8.7, $^{207}Pb/^{206}Pb$ values from 0.8315 to 0.8399, and $^{87}Sr/^{86}Sr$ values from 0.7230 to 0.7849. In the uppermost sediment samples between 115 and 43 cmbsf, the isotopic values settle approximately to the same levels as the sediments below the grey layer. The εNd values vary between -11.2 and -9.7, $^{207}Pb/^{206}Pb$ values between 0.8304 and 0.8340, and $^{87}Sr/^{86}Sr$ values between 0.7226 and 0.7406. The average isotopic values for the sediments below, in, and above the grey layer are presented in Table 1.

5. Discussion

The Eurasian source areas may have provided an ample amount of material during the MIS 4-3 transition. This enhanced sedimentation is marked by a rapid shift in core 96/12-1pc lithology to a homogeneous, dark grey, relatively coarse-grained sediment layer (Fig. 2), which correlates with various cores from the eastern and central Arctic Ocean (e.g., Vogt et al. 2001; Spielhagen et al. 2004; Dong et al. 2022). The grey layer was deposited during the MIS 4-3 transition (Jakobsson et al. 2000, 2001; Vogt et al. 2001; Spielhagen et al. 2004; Löwemark et al. 2008), and the sharp lower contact of the layer indicates an abrupt change in the sedimentation regime. The significant change in the environmental conditions within the transitional interval is reflected in the mineralogical composition of the sediments from core 96/12-1pc (e.g., Löwemark et al. 2008; Strand & Immonen 2010; Kaparulina et al. 2016) (Fig. 2).

The source areas and transportation for this MIS 4-3 transition sediment are discussed here based on the quantitative analysis of clay mineral assemblages and isotope compositions. Smectite is helpful for clay mineral provenance studies in the Arctic Ocean due to its distinct source areas. The main modern source region of smectite for the eastern/central Arctic Ocean is the shelves of the Kara Sea and the western Laptev Sea (Wahsner et al. 1999; Vogt & Knies 2008). The weathered smectite-rich material from the Siberian trap basalts (Putorana Plateau and the Siberian Platform) is transported by the Yenisey River into the Kara Sea, and by the Anabar and Khatanga rivers into the Laptev Sea (e.g., Rossak et al. 1999; Schoster et al. 2000). Higher smectite content is associated with interglacial conditions (Strand et al. 2008), and the notable increasing trend of smectite content in the grey layer (163–115 cmbsf) of core 96/12-1pc (Fig. 2) may indicate deglacial sediment transport from the retreating Eurasian ice sheet. The abrupt transition to higher kaolinite content occurs in the lower part of the grey layer (~160 cmbsf) and an excursion at the MIS 4 top (~130 cmbsf) (Fig. 2).

According to Vogt (1997), high kaolinite content in the central Arctic Ocean sediments suggests origin from the Kara Sea and the western Laptev Sea. Kaolinite is a very resistant mineral, and its occurrence in the polar regions may be derived from the reworking of older, kaolinite-bearing sediments (Darby 1975; Chamley 1989; Hambrey et al. 1991). The fluctuating kaolinite content in the studied sediments (Fig. 2) can be related to these reworked sediments and to the intensity of erosion at the continental source areas. According to Wahsner et al. (1999), increased illite content is characteristic for sediments of the eastern Laptev Sea and the East Siberian Sea. The higher illite content in the core 96/12-1pc sediment column indicates that the illite-rich IRD was derived from glacial sources. However, the decreasing illite content in the grey layer at 163–115 cmbsf (Fig. 2) implies availability of other clay minerals during deglaciation. In comparison, the chlorite content shows a slight increase in the grey layer (Fig. 2) and according to Dong et al. (2017) the elevated chlorite content is characteristic for interglacial environments. Wahsner et al. (1999) showed that chlorite distribution is relatively uniform in the Arctic Ocean surface sediments, and as reported by Rossak et al. (1999), a slightly higher chlorite component is delivered to the Laptev Sea by the Lena and Yana rivers.

The obtained sediment isotopic compositions of radiogenic Nd, Pb and Sr from core 96/12-1pc can be compared with the values of the circum-Arctic magmatic and metamorphic outcrops, as well as the rivers draining into the Arctic Ocean (Fig. 3). The Eurasian shelf sediments, which represent a mixed material drained from the vast Siberian hinterland, generally have a narrow range of Nd and Sr isotope composition (e.g., Tütken et.al. 2002; Maccali et al. 2018). The studied sediments in core 96/12-1pc overall have εNd values ranging from -8.7 to -11.4 and $^{87}Sr/^{86}Sr$ ratios between 0.719 and 0.785 (Figs. 2, 3). These values are mostly similar to the isotopic composition of the sediments from the Kara Sea (Tütken et al. 2002; Maccali et al. 2013) and western Laptev Sea (Eisenhauer et al. 1999) (Fig. 3). These shelf areas contain weathering products from the Siberian flood basalts (such as

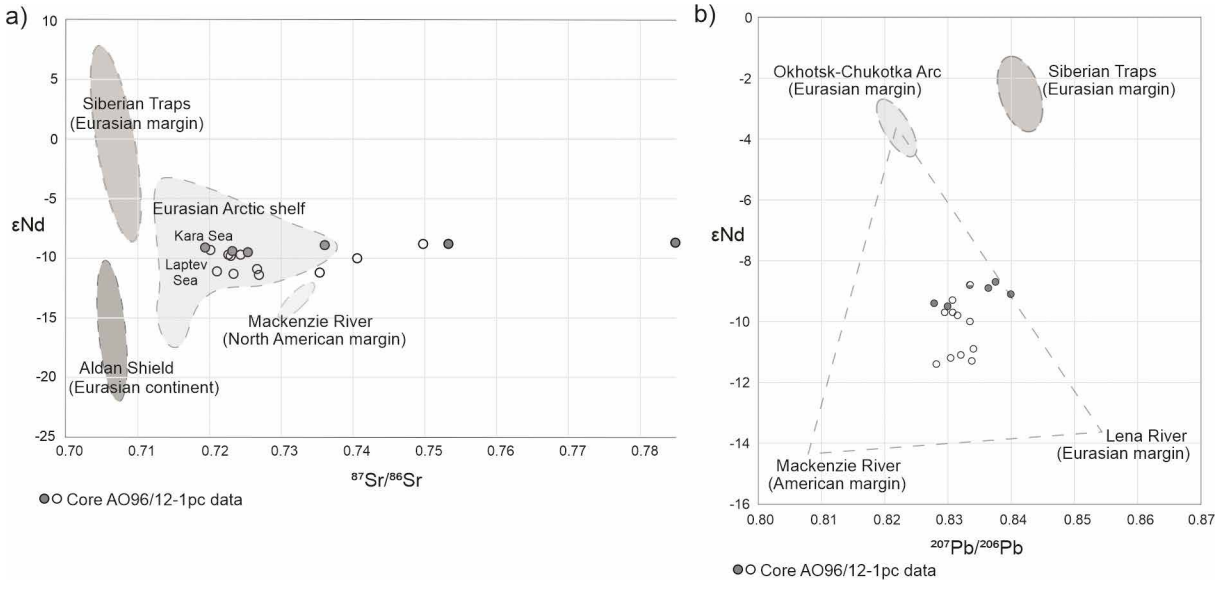

Figure 3. a) εNd vs $^{87}Sr/^{86}Sr$ diagram representing core 96/12-1pc data (white and grey circles). Grey circles indicate samples from the grey layer. The isotopic signatures of regional sources are from Siperian Traps (Lightfoot et al. 1993), Aldan Shield (Davies et al. 2006), Eurasian shelf (Eisenhauer et al. 1999, Tütken et al. 2002, Maccali et al. 2018), and Mackenzie River (Dong et al. 2020). b) Diagram of εNd vs $^{207}Pb/^{206}Pb$ representing core 96/12-1pc data (white and grey circles). Grey circles indicate samples from the grey layer. Values are plotted against the proposed endmembers for $^{207}Pb/^{206}Pb$ and εNd mixing in the Arctic Ocean (Fagel et al. 2014). The isotopic signatures of regional sources are from Fagel et al. (2014) and references therein.

the Putorana Plateau), and thus, have generally higher εNd values (around -9.0) and lower $^{87}Sr/^{86}Sr$ ratios in comparison to the eastern Laptev Sea and the East Siberian Sea fed mostly by crustal sources (e.g., Li et al. 2023). The Kara Sea and the western Laptev Sea source is evident especially in the grey layer sediments, where the radiogenic isotope composition average has clearly higher values of εNd (the highest -8.3) compared to the sediments below and above the grey layer (Table 1). The high $^{87}Sr/^{86}Sr$ ratios (>0.785) may be explained by the components derived from primitive intrusive rocks and granitoids of the Archean basement in the Siberian hinterland (Czamanske et al. 2000). As a provenance indicator, volcanic rocks are the main carriers of Nd; however, igneous rocks are normally enriched in Pb (Tütken et al. 2002). The Pb isotope compositions in several samples from the grey layer (163–115 cmbsf) have high radiogenic $^{207}Pb/^{206}Pb$ values of 0.836–0.840 (Figs. 2, 3), thus supporting the inference of sedimentary contributions from the Eurasian margin.

According to the reconstruction by Mangerud et al. (2004), the Putorana Plateau and the southern Kara Sea shelf were situated within the boundaries of an ice dammed lake that could have produced the abrupt flooding event and the voluminous discharge of sediments from these provenances. It is assumed that sediments from the Eurasian margin sources, such as the shelves of the Kara and western Laptev Sea, are mainly transported by ice via the Transpolar Drift and deposited in the Eurasian Basin (Spielhagen et al. 2004; Strand et al. 2008; Strand & Immonen 2010). The results from this study support that the sediments in the grey layer of core 96/12-1pc can be related to the disintegration of the Middle Weichselian ice sheet and the discharge of the large proglacial lake during deglaciation in the MIS 4-3 transition. The sediments deposited on the Lomonosov Ridge could have been transported during this glacial/interglacial change by icebergs, sea ice and in suspension.

6. Conclusions

Clay mineralogy analysis combined with the determination of Nd, Pb, and Sr isotopes in clay fraction were used for the interpretation of source areas and transport mechanisms of sediments from the Lomonosov Ridge in the central Arctic Ocean. The distinct changes in sediment characteristics within the grey, relatively coarse-grained sedimentary layer deposited during the MIS 4-3 transition are represented by the clay mineral assemblages and isotopic compositions. The high smectite and kaolinite content in the grey layer are probably related to weathering products of the Siberian basaltic rocks and indicate origin from the shelves of the Kara Sea and the western Laptev Sea. The Nd and Sr isotope values fall mostly within the ranges typical for these shelf areas. We conclude that the Nd, Pb and Sr isotopic compositions of sediments in the grey layer mark a pronounced deglacial impact during the MIS 4-3 transition at the end of the Middle Weichselian glaciation. An abrupt change in the sedimentation regime indicated by provenance and the deposition of a coarse IRD-rich grey layer, might be related to the discharge of an ice dammed lake in the northern Siberia from where voluminous sediment load have been transported to the Arctic Ocean by icebergs, sea ice and in suspension.

Supplementary Data

Electronic Appendices are available via Bulletin of Geological Society of Finland web page.
Electronic Appendix A: The detailed results from the clay mineralogy analysis
Electronic Appendix B: Nd, Pb and Sr isotope analyses

Acknowledgements

The core 96/12-1pc materials came from the Arctic Ocean–96 Expedition (AO96) organised by the Swedish Polar Research Secretariat in close collaboration with the Stockholm University colleagues Jan Backman and Martin Jakobsson. Discussions provided by them and Ludvig Lövemark are very much appreciated. This research was financially supported by the Academy of Finland (project No. 269182) ICE (Indexing transitions in ice sheet decay in the Eurasian Arctic marine and land record). This research is part of the University of Oulu funded project Loss of Ice in the Arctic System (LIAS): geological perspective of global environmental change. We acknowledge the staff of the Centre for Material Analysis (CMA), University of Oulu for the XRD operation and especially Heather Tessier for finalising the clay mineralogical database utilised in this paper. We thank Irmeli Mänttäri and Yann Lahaye from the Finnish Geosciences Research Laboratory at the Geological Survey of Finland, Espoo where the TIMS and MC-ICP-MS analysis were performed. We also thank Professor Tapani Rämö from the University of Helsinki for helping in the neodymium analysis. We thank Ropert Spielhagen and Leonid Polyak for their constructive improvements and useful comments on the manuscript.

References

AMAP Assessment Report: Arctic Pollution Issues, 1998. Figure 3.29. http://www.amap.no/documents/doc/amap-assessment-report-arctic-pollution-issues/68

Adler, R.E., Polyak, L., Ortiz, J.D., Kaufman, D.S., Channell, J.E.T., Xuan, C., Grottoli, A.G., Sellen, E. & Crawford, K.A.2009. Sediment record from the western Arctic Ocean with an improved Late Quaternary age resolution: HOTRAX core HLY0503-8JPC, Mendeleev Ridge. Global and Planetary Change 68, 18–29. https://doi.org/10.1016/j.gloplacha.2009.03.026

Biscaye, P. E., 1965. Mineralogy and sedimentation of recent deep-sea clays in the Atlantic Ocean and adjacent oceans. Geological Society of America Bulletin 76, 803–832. https://doi.org/10.1130/0016-7606(1965)76[803:MASORD]2.0.CO;2

Chamley, H., 1989. Clay Sedimentology. Springer Verlag, Berlin, 623 p.

Clark, D.L. & Hanson, A., 1983. Cetral Arctic Ocean Sediment Texture: A Key to Ice Transport Mechanisms. In: Molnia, B.F. (eds.) Glacial-Marine Sedimentation. Springer, Boston, MA. https://doi.org/10.1007/978-1-46-13-3793-5_7

Czamanske, G.K., Wooden, J.L., Walker, R.J., Fedorenko, V.A., Simonov, O.N., Budahn, J.R. & Siems, D.F., 2010. Geochemical, Isotopic, and SHRIMP Age Data for Precambrian Basement Rocks, Permian Volcanic Rocks, and Sedimentary Host Rocks to the Ore-bearing Intrusions, Noril'sk-Talnakh District, Siberian Russia. International Geology Review 42, 895–927. https://doi.org/10.1080/00206810009465117

Darby, D.A., 1975. Kaolinite and other clay minerals in Arctic Ocean sediments. Journal of Sedimentary Research 45, 272–279. https://doi.org/10.1306/212F6D34-2B24-11D7-8648000102C1865D

Darby, D.A., 2003. Sources of sediment found in sea ice from the western Arctic Ocean, new insights into processes of entrainment and drift patterns. Journal of Geophysical Research: Oceans 108, C8. https://doi.org/10.1029/2002JC001350

Darby, D.A., 2014. Ephemeral formation of perennial sea ice in the Arctic Ocean during the middle Eocene. Nature Geoscience 7, 210–213. https://doi.org/10.1038/ngeo2068

Darby, D.A., Myers, W.B., Jakobsson, M. & Rigor, I., 2011. Modern dirty sea ice characteristics and sources: The role of anchor ice. Journal of Geophysical Research: Oceans 116, C9. https://doi.org/10.1029/2010JC006675

Davies, G.R, Stolz, A.J, Mahotkin, I.L., Nowell, G.M. & Pearson, D.G., 2006. Trace element and Sr-Pb-Nd-Hf isotope evidence for ancient, fluid-dominated enrichment of the source of Aldan shield lamproites. Journal of Petrology 47, 1119–1146. https://doi.org/10.1093/petrology/egl005

DePaolo, D.J. & Wasserburg, G.J., 1976. Inferences about Magma Sources and Mantle Structure from Variations of $^{143}Nd/^{144}Nd$. Geophysical Research Letters 3, 743–746. https://doi.org/10.1029/GL003i012p00743

Dong, L., Liu, Y., Shi, X., Polyak, L., Huang, Y., Fang, X., Liu, J., Zou, J., Wang, K., Sun, F. & Wang, X., 2017. Sedimentary record from the Canada Basin, Arctic Ocean: implications for the late to middle Pleistocene glacial history. Climate of the Past, 13, 511–531. https://doi.org/10.5194/cp-13-511-2017

Dong, L., Polyak, L., Liu, Y., Shi, X., Zhang, J. & Huang, Y., 2020. Isotopic fingerprints of ice-rafted debris offer new constraints on Middle to Late Quaternary Arctic circulation and glacial history. Geochemistry, Geophysics, Geosystems 21, e2020GC00901. https://doi.org/10.1029/2020GC009019

Dong, L., Polyak, L., Xiao, X., Brachfeld, S., Liu, Y., Shi, X., Fang, X., Bai, Y., Zhu, A., Li, C., Zhao, S., Wu, D. &

Wang, C., 2022. A Eurasian Basin sedimentary record of glacial impact on the central Arctic Ocean during MIS 1–4. Global and Planetary Change 219, 103993. https://doi.org/10.1016/j.gloplacha.2022.103993

Eisenhauer A., Meyer, H., Rachold, V., Tütken, T., Wiegand, B., Hansen, B.T., Spielhagen, R.F., Lindemann, F. & Kassens, H., 1999. Grain size separation and sediment mixing in Arctic Ocean sediments: evidence from the strontium isotope systematic. Chemical Geology 158, 173–188. https://doi.org/10.1016/S0009-2541(99)00026-1

Fagel, N., Not, C., Gueibe, J., Mattielli, N. & Bazhenova, E., 2014. Late Quaternary evolution of sediment provenances in the Central Arctic Ocean: Mineral assemblage, trace element composition and Nd and Pb isotope fingerprints of detrital fraction from the Northern Mendeleev ridge.Quaternary Science Reviews 92, 140–154. https://doi.org/10.1016/j.quascirev.2013.12.011

Hambrey, M.J., Ehrmann, W. & Larsen, B., 1991. Cenozoic glacial record of the Prydz Bay continental shelf, East Antarctica. In: Barron, J., Larsen, B., et al. (eds.), Proc. ODP, Sci. Results, College Station, TX. (Ocean Drilling Program) 119, 77–132. doi:10.2973/odp.proc.sr.119.200.1991

Hardy, R. & Tucker, M., 1988. X-ray powder diffraction of sediments. In: Tucker, M. (Ed), Techniques in Sedimentology. Blackwell, Oxford, 191–228.

Jakobsson, M., Løvlie, R., Al-Hanbali, H., Arnold, E., Backman, J. & Morth, M., 2000. Manganese and color cycles in Arctic Ocean sediments constrain Pleistocene chronology. Geology 28, 23–26. https://doi.org/10.1130/0091-7613(2000)28<23:MACCIA>2.0.CO;2

Jakobsson, M., Løvlie, R., Arnold, E.M., Backman, J., Polyak, L., Knutsen, J.-O. & Musatov, E., 2001. Pleistocene stratigraphy and paleoenvironmental variation from Lomonosov Ridge sediments, central Arctic Ocean. Global and Planetary Change 31, 1–22. https://doi.org/10.1016/S0921-8181(01)00110-2

Jakobsson, M., Macnab, R., Mayer, L., Anderson, R., Edwards, M., Hatzky, J., Schenke, H.W. & Johnson, P., 2008. An improved bathymetric portrayal of the Arctic Ocean: Implications for ocean modeling and geological, geophysical and oceanographic analyses. Geophysical Research Letters 35, L07602. https://doi.org/10.1029/2008GL033520

Jokat, W. & Ickrath, M., 2015. Structure of ridges and basins off East Siberia along 81°N, Arctic Ocean. Marine and Petroleum Geology 64, 222–232. http://dx.doi.org/10.1016/j.marpetgeo.2015.02.047

Kalinenko, V.V., 2001. Clay minerals in sediments of the Arctic seas. Lithology and Mineral Resources 36, 362–372. https://doi.org/10.1023/A:101041305264

Kaparulina, E., Strand, K. & Lunkka, J.P., 2016. Provenance analysis of central Arctic Ocean sediments: Implications for circum-Arctic ice sheet dynamics and ocean circulation during Late Pleistocene. Quaternary Science Reviews 147, 210–220. http://dx.doi.org/10.1016/j.quascirev.2015.09.017

Krinner, G., Mangerud, J., Jakobsson, M., Crucifix, M., Ritz, C. & Svendsen, J.I., 2004. Enhanced ice sheet growth in Eurasia owing to adjacent ice-dammed lakes. Nature 427, 429–432. https://doi.org/10.1038/nature02233

Krylov, A.A., Andreeva, I.A., Vogt, C., Backman, J., Krupskaya, V.V., Grikurov, G.E., Moran, K. & Shoji, H., 2008. A shift in heavy and clay mineral provenance indicates a middle Miocene onset of a perennial sea ice cover in the Arctic Ocean. Paleoceanography 23, PA1S06. https://doi.org/10.1029/2007PA001497

Krylov, A.A., Stein, R. & Ermakova, L.A., 2014. Clay minerals as indicators of late quaternary sedimentation constraints in the Mendeleev Rise, Amerasian Basin, Arctic Ocean. Lithology and Mineral Resources 49, 103–116. https://doi.org/10.1134/S0024490213060059

Li, Q., Qiao, S., Shi, X., Chen, Y., Astakhov, A., Zhang, H., Hu, L., Yang, G., Bosin, A., Vasilenko, Y. & Dong, L., 2023. Sr, Nd, and Pb isotope provenance of surface sediments on the East Siberian Arctic Shelf and implications for transport pathways. Chemical Geology 618, 121277. https://doi.org/10.1016/j.chemgeo.2022.121277

Lightfoot, P.C., Hawkesworth, C.J., Hergt, J., Naldrett, A.J., Gorbachev, N.S., Fedorenko, V.A. & Doherty, W., 1993. Remobilisation of the continental lithosphere by a mantle plume: major-, trace-element, and Sr-, Nd-, and Pb-isotope evidence from picritic and tholeiitic lavas of the Noril'sk District, Siberian Trap, Russia. Contributions to Mineralogy and Petrology 114, 171–188. https://doi.org/10.1007/BF00307754

Löwemark, L., Jakobsson, M., Mörth, M. & Backman, J., 2008. Arctic Ocean manganese contents and sediment colour cycles. Polar Research 27, 105–113. http://dx.doi.org/10.1111/j.1751-8369.2008.00055.x

Maccali, J., Hillaire-Marcel, C., Carignan, J. & Reisberg, L.C., 2013. Geochemical signatures of sediments documenting Arctic sea-ice and water mass export through Fram Strait since the Last Glacial Maximum. Quaternary Science Reviews 64, 136–151. http://dx.doi.org/10.1016/j.quascirev.2012.10.029

Maccali, J., Hillaire-Marcel, C. & Not, C., 2018. Radiogenicisotope (Nd, Pb, Sr) signatures of surface and sea ice-transported sediments from the Arctic Ocean under the present interglacial conditions. Polar Research 37, 1442982. https://doi.org/10.1080/17518369.2018.1442982

Mangerud, J., Astakhov, V., Jakobsson, M. & Svedesn, J.I., 2001. Huge ice-age lakes in Russia. Journal of Quaternary Science 16, 773–777. https://doi.org/10.1002/jqs.661

Mangerud, J., Jakobsson, M., Alexanderson, H., Astakov, V., Clarke, G., Henriksen, M., Hjort, C., Krinner, G., Lunkka, J.P., Moller, P., Murray, A., Nikolskaya, O., Saarnisto, M. & Svendsen, J.I., 2004. Ice-dammed lakes and rerouting of the drainage of Northern Eurasia during the last glaciation. Quaternary Science Reviews 23, 1313–1332. https://doi.org./10.1016/jquascirev.2003.12.009

Moore, D. M. & Reynolds Jr., R. C., 1997. X-ray Diffraction and the Identification and Analysis of Clay Minerals (2nd edition). Oxford University Press, Oxford, 378 p.

Polyak, L., Alley, R.B., Andrews, J.T., Brigham-Grette, J., Cronin, T.M., Darby, D.A., Dyke, A.S., Fitzpatrick, J.J., Funder, S., Holland, M., Jennings, A.E., Miller, G.H., O'Regan, M., Savelle, J., Serreze, M., St. John, K., White, J.W.C. & Wolff, E., 2010. History of sea ice in the Arctic. Quaternary Science Reviews 29, 1757–1778. https://doi.org/10.1016/j.quascirev.2010.02.010

Richard, P., Shimizu, N. & Allègre, C.J., 1976. $^{143}Nd/^{146}Nd$, a Natural Tracer: An Application to Oceanic Basalts. Earth and Planetary Science Letters 31, 269–278. https://doi.org/10.1016/0012-821X(76)90219-3

Rossak, B.T., Kassens, H., Lange, H. & Thiede, J., 1999. Clay Mineral Distribution in Surface Sediments of the Laptev Sea: Indicator for Sediment Provinces, Dynamics and Sources. In: Land-Ocean Systems in the Siberian Arctic. Springer, Berlin, Heidelberg, pp. 587–599. https://doi.org/10.1007/978-3-642-60134-7_45

Schoster, F., Behrends, M., Müller, C., Stein, R. & Wahsner, M., 2000. Modern river discharge and pathways of supplied material in the Eurasian Arctic Ocean: evidence from mineral assemblages and major and minor element distribution. International Journal of Earth Sciences 89, 486–495. https://doi.org/10.1007/s005310000120

Spielhagen, R.F., Baumann, K-H., Erlenkeuser, H., Nowaczyk, N.R., Nørgaard-Pedersen, N., Vogt, C. & Weiel, D., 2004. Arctic Ocean deep-sea record of northern Eurasian ice sheet history. Quaternary Science Reviews 23, 1455–1483. https://doi.org/10.1016/j.quascirev.2003.12.015

Stein, R., Grobe, H. & Wahsner, M., 1994. Organic carbon, carbonate, and clay mineral distributions in eastern central Arctic Ocean surface sediments. Marine Geology 119, 269–285. https://doi.org/10.1016/0025-3227(94)90185-6

Strand, K., Junttila, J., Lahtinen, T. & Turunen, S., 2008. Climatic transitions in the Arctic as revealed by mineralogical evidence from the Upper Cenozoic sediments in the central Arctic Ocean and the Yermak Plateau. Norsk Geologisk Tidsskrift 88, 305–312.

Strand, K. & Immonen, N., 2010. Dynamics of the Barents-Kara Ice Sheet as revealed by quartz sand grain microtextures of the late Pleistocene Arctic Ocean sediments. Quaternary Science Reviews 29, 3583–3589. https://doi.org/10.1016/j.quascirev.2010.09.017

Svendsen, J.I., Alexanderson, H., Astakhov, V.I., Demidov, I., Dowdeswell, J.A., Funder, S., Gataullin, V., Henriksen, M., Hjort, C., Houmark-Nielsen, M., Hubberten, H.W., Ing Ólfsson, Ó., Jakobsson, M., Kjær, K.H., Larsen, E., Lokrantz, H., Lunkka, J.P., Lysså, A., Mangerud, J., Matiouchkov, A., Murray, A., Möller, P., Niessen, F., Nikolskaya, O., Polyak, L., Saarnisto, M., Siegert, C., Siegert, M.J., Spielhagen, R.F. & Stein, R., 2004. Late Quaternary ice sheet history of northern Eurasia. Quaternary Science Reviews 23, 1229–1271. https://doi.org/10.1016/j.quascirev.2003.12.008

Tütken T., Eisenhauer A., Wiegand B. & Hansen B.T., 2002. Glacial–interglacial cycles in Sr and Nd isotopic composition of Arctic marine sediments triggered by the Svalbard/Barents Sea ice sheet. Marine Geology 182, 351–372. https://doi.org/10.1016/S0025-3227(01)00248-1

Velde, B., 1992. Introduction to Clay Minerals: Chemistry, Origins, Uses and Environmental Significance. London. Chapman & Hall, 198 p.

Viscosi-Shirley, C., Mammone, K., Pisias, N. & Dymond, J., 2003. Clay mineralogy and multi-element chemistry of surface sediments on the Siberian Arctic shelf: Implications for sediment provenance and grain size sorting. Continental Shelf Research 23, 1175–1200. https://doi.org/10.1016/S0278-4343(03)00091-8

Vogt, C., 1997. Regional and temporal variations of mineral assemblages in Arctic Ocean sediments as climatic indicator during glacial/interglacial changes. Ber. Polarforsch. 251, 309 p.

Vogt, C., Knies, J., Spielhagen, R.F. & Stein, R., 2001. Detailed mineralogical evidence for two nearly identical glacial/deglacial cycles and Atlantic water advection to the Arctic Ocean during the last 90,000 years. Global and Planetary Change 31, 23–44. https://doi.org/10.1016/S0921-8181(01)00111-4

Vogt, C. & Knies, J., 2008. Sediment dynamics in the Eurasian Arctic Ocean during the last deglaciation: the clay mineral group smectite perspective. Marine Geology 250, 211–222. https://doi.org/10.1016/j.margeo.2008.01.006

Wahsner, M., Müller, C., Ivanov, G., Nürnberg, D., Shelekhova, E.S., Stein, R. & Tarasov, G., 1999. Clay mineral distributions in surface sediments from Eurasian Arctic Ocean and the Eurasian continental margin as indicator for source areas and transport pathways of sediments: A synthesis, Boreas 28, 215–233. https://doi.org/10.1111/j.1502-3885.1999.tb00216.x

Yuan, H., Yuan, W., Cheng, C., Liang, P., Liu, X., Dai, M., Bao, Z., Zong, C., Chen, K. & Lai, S., 2016. Evaluation of lead isotope compositions of NIST NBS 981 measured by thermal ionization mass spectrometer and multiple-collector inductively coupled plasma mass spectrometer. Solid Earth Sciences 1, 74–78. http://dx.doi.org/10.1016/j.sesci.2016.04.001